

Motion of proximal histidine and structural allosteric transition in soluble guanylate cyclase

 Byung-Kuk Yoo^a, Isabelle Lamarre^a, Jean-Louis Martin^a, Fabrice Rappaport^b, and Michel Negrier^{a,1}
^aLaboratoire d'Optique et Biosciences, INSERM U1182, Ecole Polytechnique, 91128 Palaiseau Cedex, France; and ^bLaboratoire de Physiologie Membranaire et Moléculaire du Chloroplaste, UMR7141, Institut de Biologie Physico-Chimie, 75005 Paris, France

Edited by William A. Eaton, National Institute of Diabetes and Digestive and Kidney Diseases, National Institutes of Health, Bethesda, MD, and approved March 2, 2015 (received for review December 3, 2014)

We investigated the changes of heme coordination in purified soluble guanylate cyclase (sGC) by time-resolved spectroscopy in a time range encompassing 11 orders of magnitude (from 1 ps to 0.2 s). After dissociation, NO either recombines geminately to the 4-coordinate (4c) heme ($\tau_{G1} = 7.5$ ps; 97 ± 1% of the population) or exits the heme pocket (3 ± 1%). The proximal His rebinds to the 4c heme with a 70-ps time constant. Then, NO is distributed in two approximately equal populations (1.5%). One geminately rebinds to the 5c heme ($\tau_{G2} = 6.5$ ns), whereas the other diffuses out to the solution, from where it rebinds bimolecularly ($\tau = 50$ μs with [NO] = 200 μM) forming a 6c heme with a diffusion-limited rate constant of 2×10^8 M⁻¹·s⁻¹. In both cases, the rebinding of NO induces the cleavage of the Fe-His bond that can be observed as an individual reaction step. Saliiently, the time constant of bond cleavage differs depending on whether NO binds geminately or from solution ($\tau_{5C1} = 0.66$ μs and $\tau_{5C2} = 10$ ms, respectively). Because the same event occurs with rates separated by four orders of magnitude, this measurement implies that sGC is in different structural states in both cases, having different strain exerted on the Fe-His bond. We show here that this structural allosteric transition takes place in the range 1–50 μs. In this context, the detection of NO binding to the proximal side of sGC heme is discussed.

soluble guanylate cyclase | nitric oxide | time-resolved absorption spectroscopy | allostery | protein activation

The soluble guanylate cyclase (sGC), localized in many different cell types, is the receptor of the endogenous messenger nitric oxide (NO) and catalyzes the formation of cGMP from GTP upon activation triggered by NO binding (1, 2). The diatomic messenger NO and sGC play a critical role in several physiological processes: regulation of vascular blood pressure and cardiovascular diseases (3), lung airway relaxation and pulmonary pathologies (4), immune response and inflammatory disorders (5), and tumor progression and apoptosis (6). Thus, sGC is a pharmacological target of very high interest, and several activators have been developed (7, 8), leading to the approval of riociguat for the treatment of pulmonary hypertension (9, 10). Because of its pharmacological interest, the mechanisms of activation, deactivation, and regulation of sGC must be deciphered at the molecular level. Despite numerous efforts, the 3D crystal structure of heterodimeric sGC remains unknown, but the heme domain of the sGC β1-subunit [called heme NO/oxygen-binding (H-NOX)] was modeled from the heme domain of bacterial NO sensors (11, 12) and the sGC catalytic α1-subunit was modeled from the catalytic α1-subunit of adenylate cyclase (13). Recently, the entire quaternary structure of sGC was reconstructed by inserting individual protein domains into the density envelope of entire single-sGC molecules observed by EM (14), revealing a high flexibility of the sGC dimer. Subsequently, the structural perturbations induced by NO binding were mapped at the domain interfaces (15). In the past decade, a diversity of molecular models and regulatory models have been proposed (16–23), with some including structural hypotheses and involving or not involving the hypothetical NO binding to the proximal heme side (vs. distal NO binding).

The heterodimeric sGC (~150 kDa) comprises a regulatory domain in the β-subunit that contains the prosthetic heme group for NO binding, which activates the synthesis of cGMP from GTP, whereas the interface between the C termini of both α- and β-subunits harbors the GTP-binding catalytic site, remote from the heme domain (Fig. 1). The first internal molecular event correlated with sGC activation is the cleavage of the heme-proximal His covalent bond induced by NO binding (24). This event triggers the structural allosteric changes within the protein that induce the increase of catalytic activity. Because the sensing heme domain and the catalytic site are separated by a helical domain (15), there are necessary structural changes for “cross-talk” between both, mediating the allosteric regulation. The NO concentration dependence of NO binding (16) and the modulation of the sGC activity by nucleotides (21), together with the possibility of its activation by artificial compounds (7), illustrate the complexity of sGC regulation when interacting with its messenger NO.

One critical aspect for understanding this allosteric mechanism is the identification of structural transitions and intermediate species, which must be addressed by time-resolved techniques. We have previously observed that after NO dissociation from the heme (25, 26), NO recombines geminately to the reactive 4-coordinate (4c) heme with a very high probability (97% of dissociated NO with time constant $\tau = 7.5$ ps). However, the dynamics of the 3% NO population that does not rebind geminately have not been identified so far. Here, we focused on the transitions occurring after NO has left the heme pocket of sGC. We investigated the dynamics of the heme coordination by time-resolved absorption spectroscopy in a time range

Significance

Soluble guanylate cyclase is the mammalian endogenous nitric oxide (NO) receptor that controls numerous signaling physiological processes. Time-resolved spectroscopy allowed us to probe the dynamics of the heme coordination after NO release and binding. After photodissociation of NO, all heme transitions are identified within the time range of 1 ps to 0.2 s, notably the bond breaking and reformation between the heme iron and proximal His, which are major events for the activation/deactivation processes. It is thus possible to demonstrate that the structural allosteric transition occurs in the time range 1–50 μs, which remarkably matches the time range observed for hemoglobin, the prototypic protein for allostery. These findings relate not only to NO signaling but also to general allostery in heme proteins.

Author contributions: M.N. designed research; B.-K.Y., I.L., F.R., and M.N. performed research; B.-K.Y., F.R., and M.N. analyzed data; and J.-L.M., F.R., and M.N. wrote the paper.

The authors declare no conflict of interest.

This article is a PNAS Direct Submission.

¹To whom correspondence should be addressed. Email: michel.negrier@polytechnique.fr.

 This article contains supporting information online at www.pnas.org/lookup/suppl/doi:10.1073/pnas.1423098112/-DCSupplemental.

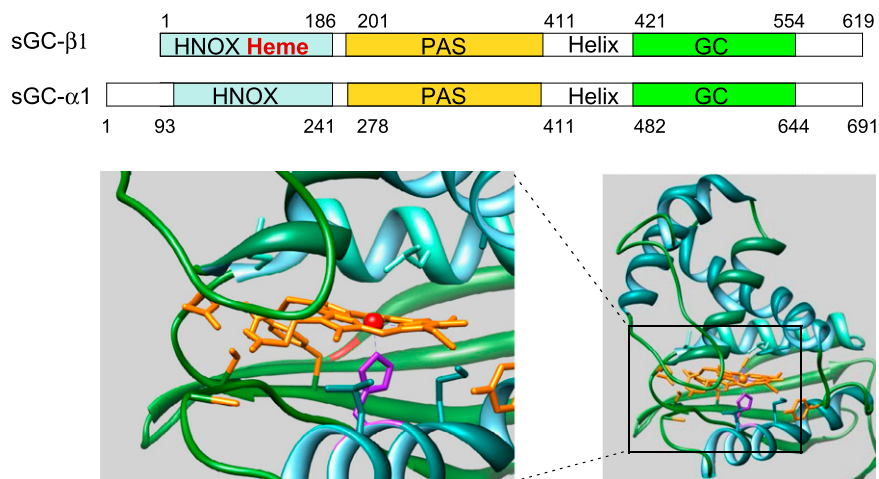


Fig. 1. Sequence domain organization of sGC and focus on the structure of the heme-sensing domain. GC, guanylate cyclase; PAS, period circadian protein-aryl hydrocarbon receptor-single minded protein.

encompassing 11 orders of magnitude, from 1 ps to 0.2 s. Methodologically, the photodissociation of the ligand NO from the heme with a fast laser pulse allows one to displace the equilibrium and to simulate the thermal release of NO. Then, because NO can either rebind immediately from within the heme pocket or migrate within the protein core and eventually to the

solution, from where it may rebind at a longer time, we could monitor each of the intermediate states of the heme during the dynamics of NO from the solution to the heme by exploring 11 time decades. We report the heme iron coordination dynamics triggered by NO release and binding, and we have identified the subsequent transitions, including the time range

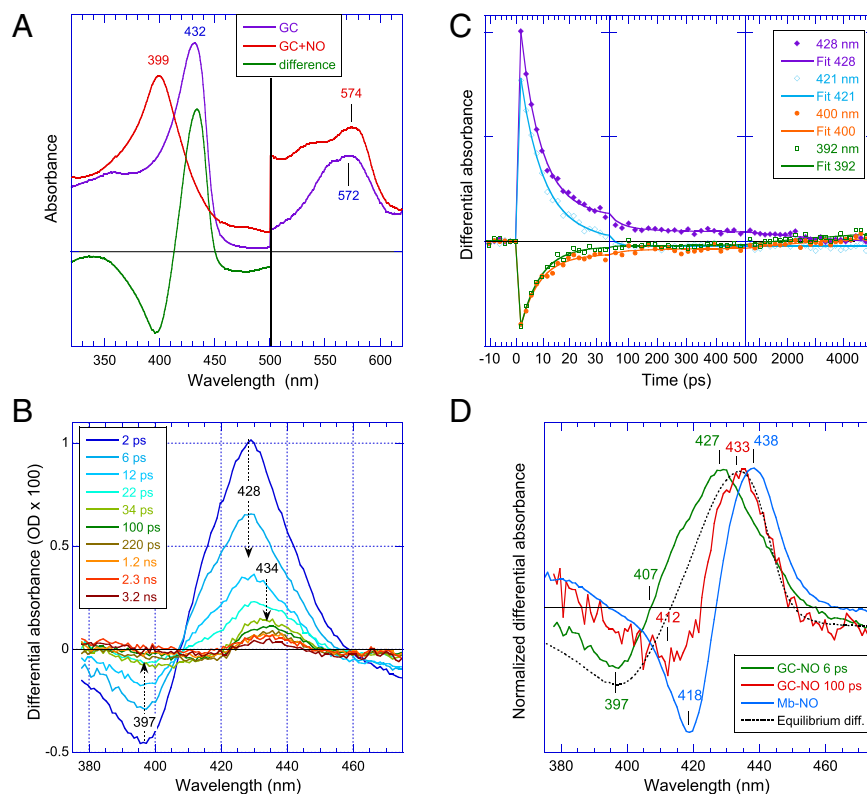


Fig. 2. Picosecond to 5-ns dynamics after NO dissociation. (A) Equilibrium spectra of unliganded 5c-His sGC and nitrosylated 5c-NO sGC. (B) Raw transient spectra at indicated time delays. (C) Raw kinetics up to 5 ns at indicated wavelengths, fitted to a sum of three exponential components yielding the time constants in Table S1. The averaged time constants were $\tau_1 = 7.5 \pm 0.5$ ps, $\tau_2 = 70 \pm 10$ ps, and $\tau_3 = 5,600 \pm 500$ ps. In the three windows, the time intervals between transient spectra were 2 ps, 22.5 ps, and 180 ps, respectively. Because of the 2-ps time interval in the first window, it was not necessary to add a fourth component to take into account the excited state decay of the heme, which is usually $\tau_{ex} = 2.5\text{--}3.5$ ps. (D) Comparison of normalized transient spectra at +6 ps and +100 ps after NO dissociation, with the equilibrium difference (5c-His minus 5c-NO) revealing the difference in transient processes. The equilibrium difference with 6c-NO myoglobin is also compared. diff., difference.

of the allosteric transition between the activated and resting states of sGC.

Results

Rebinding of Proximal His to the 4c Heme After NO Release from the Heme Pocket. We first recorded the heme dynamics after NO photodissociation on a 5-ns time scale with a subpicosecond resolution (Fig. 2). After addition of NO into the cuvette, sGC becomes 5c-NO within seconds (16, 27) and no 6c-NO heme remains (Fig. 2A). This 5c-NO species is the starting state in our measurements. The dissociation of NO yields a 4c heme, as observed by the bleaching at 397 nm (Fig. 2B) to which NO geminately rebinds without energy barrier from within the heme pocket with $\tau_{\text{gem}} = 7.5$ ps (25, 26), a property observed in other 4c heme proteins (28, 29). Accordingly, the induced absorption centered at 428 nm due to the 4c heme decreases rapidly, and a new maximum appears, centered at 433 nm, meaning that a second species was formed and decays more slowly.

The kinetics at specific and discrete wavelengths (Fig. 2C) were fitted to obtain the time constants (Table S1). Because a single exponential did not yield a satisfactory fit, we used a sum of two or three exponential terms, and the dependence of their amplitudes upon the wavelength allowed the assignment of the transitions to specific processes. The evolution of transient spectra (Fig. 2B) clearly discloses a shift of induced absorption from 428 to 433 nm. The comparison of difference transient spectra at +6 ps and +100 ps (Fig. 2D) readily differentiates NO rebinding and His rebinding, both to the 4c heme. The spectrum at +100 ps discloses bleaching centered at 412 nm that corresponds to the blue side of the absorption spectrum of 4c heme, whereas its induced absorption at 433 nm is due to the 5c-His heme, as inferred from the overlap of its edge with the steady-state difference above 430 nm (Fig. 2D). Therefore, the transient spectrum at +100 ps is assigned to the rebinding of the proximal His (His¹⁰⁵) to the 4c heme, exactly as we have observed in the case of the bacterial NO-binding cytochrome *c'* (30). This rebinding occurs with a time constant $\tau_{\text{His}} = 70 \pm 10$ ps, one order of magnitude larger than NO geminate rebinding. Importantly, the recovery of the 5c-His state of heterodimeric sGC should not be interpreted as a fully relaxed protein because structural changes between subunits take place on a much slower time scale (Discussion).

Are there components slower than NO geminate and His rebinding dynamics? Indeed, the induced absorption centered at 433 nm further decays up to 5 ns with a third time constant fitted to $\tau_3 = 5.6 \pm 0.6$ ns (Table S1). It is loosely defined here because it is similar to the measured time scale (but see below). Because the Fe-His has been reformed, we assign this decay to NO rebinding to the 5c-His. However, this time constant is much larger than those time constants measured for geminate rebinding of NO to 5c-His from within the heme pocket of myoglobin, hemoglobin, and dehaloperoxidase (31). In sGC, NO is expected to have already escaped the heme pocket after several nanoseconds but not to have diffused to the solvent, so that τ_3 must reflect rebinding from the protein core.

Nanosecond to Second Dynamics After NO Dissociation: NO Rebinding Phases and Heme Iron-His Bond Cleavage. The above observation that 4c heme does not remain after ~ 100 ps and that a small amount (~ 1.5 – 2%) of 5c-His has been reformed, to which NO may rebind geminately, prompted us to investigate the subsequent heme transitions possibly occurring in a broader time range. Because the population to be probed is very small (3–4%) with respect to the initially photodissociated nitrosylated sGC population, we have used a spectroscopic system (32) that ensures the detection of signal variations as low as $\Delta\text{OD}/\text{OD} < 10^{-5}$.

The kinetics in a very broad time range (from 1 ns to 0.2 s; Fig. 3A) at eight different wavelengths first display a peak whose

intensity is higher at 435 nm and which corresponds to the fast formation of 5c-His sGC after NO photodissociation. This assignment is supported by the transient signature of the initial peak, whose maximum absorbance among the eight kinetics is located at 435 nm. The initial rise of the signal is due to the convolution of the 6-ns laser pulse with the protein response upon NO photodissociation within the pulse width and is the same at any wavelengths and for any protein (Fig. S1). It must be emphasized that because the NO geminate recombination to the 4c heme is ultrafast ($\tau_{\text{gem}} = 7.5$ ps), numerous cycles of photodissociation/recombination can occur for the same molecules during the 6-ns pulse used. This phenomenon, already observed for cytochrome *c'* (28, 33), results in a higher apparent dissociation yield so that kinetics in subsequent decades appear with a higher amplitude relative to the initial peak than in measurements using a femtosecond excitation pulse (Fig. 2C). This larger yield is an advantage for detecting the small signal that remains at 5 ns, as observed in the previous time range (1 ps to 5 ns), so that we can clearly separate all transitions in these kinetics. The repetitive dissociation/recombination cycles induce an initial peak response that contains both NO dissociation and His¹⁰⁵ rebinding, which thus leads to a larger population of reformed 5c-His species. We note that exciting the protein with a 6-ns pulse may only increase the probability of NO dissociation and that the 532-nm pulse is subsaturating. It does not induce a large excess of energy in the heme once the ligand is dissociated, and the thermal relaxation of the heme occurs rapidly in ~ 4 ps (25) without interfering with the physiologically relevant processes. Furthermore, by exciting the 5c-His sGC in the absence of NO, we have verified that the dissociating pulse at 532 nm cannot induce the photodissociation of the proximal His (25), and thus cannot perturb the physiological His dynamics. The temporal profile of the initial peak, which is the convolution of excitation and probe pulses, was fitted to a Gaussian function whose width is the width of the laser pulses (Fig. 3B), and the maximum of this Gaussian determines the time origin in the subsequent analysis in Fig. 3 C and D.

After $\Delta t = +3$ ns following the peak maximum, a decay departs from the temporal profile of the Gaussian pulse shape, which is easily distinguished at wavelengths of 430–445 nm (Fig. 3 B and C). This starting decay is simultaneous to an absorbance increase at wavelengths of 410–420 nm (Fig. 3D) and is followed by a complex evolution of the signal. The kinetics after the initial pulse were globally fitted to a sum of four exponential components (obvious at 410–420 nm), as indicated in Fig. 3 C and D, corresponding to transitions of the heme coordination. All of the parameters of the fits are indicated in Table S2.

The first transition, with time constant $\tau_1 = 6.5 \pm 1$ ns, discloses simultaneously a pronounced decay at 430–445 nm due to the disappearance of 5c-His heme and an absorbance increase at 410–420 nm due to the appearance of 6c-NO heme. We therefore assigned this transition to geminate rebinding of NO present within the protein core to reformed 5c-His heme accumulated during the excitation pulse. This transition, seen here as a steep slope, has a spectral signature corresponding to the spectral signature observed on the previous time scale as a long-tailing slope with $\tau = 5.6$ ns and a small amplitude (Fig. 2C). Both the time constant and spectral feature measured for this transition, assigned to NO geminate rebinding in 5c-His \rightarrow 6c-NO, nicely agree between the picosecond-nanosecond (ps-ns) and nanosecond-millisecond (ns-ms) datasets. We can reliably connect the sequence of events observed in the ps-ns time scale with the sequence of events observed in the ns-microsecond-ms time scale despite the different photodissociation yields in both cases.

The following transition discloses simultaneous decays at 430–445 nm (less pronounced than in the preceding one) and at 410–420 nm, which are diagnostic of the disappearance of 6c-NO heme earlier formed with τ_1 . It follows NO binding in the se-

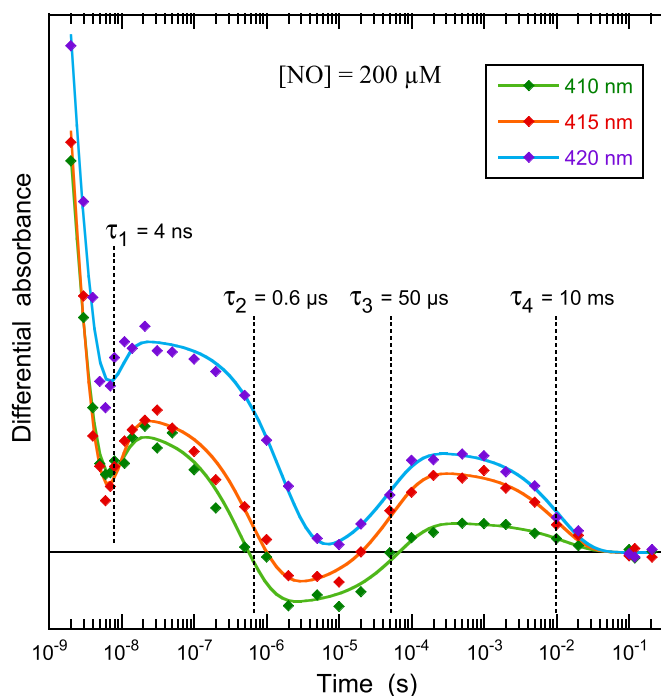


Fig. 4. Nanosecond to second dynamics of heme coordination in sGC after NO photodissociation with $[\text{NO}] = 200 \mu\text{M}$ [10% (vol/vol) in gas phase] at three particular wavelengths, where the 6c-NO species can be detected.

that nicely agree with the value measured by stopped flow ($1.0 \pm 0.3 \times 10^6 \text{ M}^{-1} \cdot \text{s}^{-1}$) (34). Contrastingly, the time constants τ_1 and τ_2 are not changed by the increased NO concentration within the experimental error, in agreement with our assignment to the geminate NO rebinding process.

Saliently, we found that the same coordination change, namely, the conversion of 6c-NO \rightarrow 5c-NO, can take place with two very different time constants ($\tau_2 = 0.6 \mu\text{s}$ and $\tau_4 = 10 \text{ ms}$). These transitions were observed as individual steps not kinetically limited by a preceding structural event, implying that we observed two different conformational states of the 6c-NO species. This observation calls for the occurrence of a structural relaxation, which is discussed below.

Discussion

Heme Transition Phases, NO Dynamics, and Consequences of His Rebinding. All of the observed transitions are listed in the Table 1, together with their corresponding rates. This complete identifica-

tion allows us to picture the full sequence of individual transitions, from photodissociation of NO to its rebinding from solvent and the reformation of the 5c-NO activated state, which has several implications that we discuss now. First, following photodissociation of NO, only two transitions take place in the picosecond range, the rebinding of either NO or His¹⁰⁵ to the 4c heme with very fast rates. The very fast rebinding of His¹⁰⁵ ($\tau_{\text{His}} = 70 \text{ ps}$) closes the proximal site, and thereby absolutely prevents the binding to the 4c heme of NO diffusing from the solution in the upper microsecond range. This phenomenon rules out that NO binding to the 4c heme depends upon NO concentration, as proposed in some models (36). Any subsequent slower geminate rebinding of NO ($>100 \text{ ps}$) must involve the 5c-His heme lead to the 6c heme with NO bound to the distal side (as occurs for bimolecular rebinding). This event is precisely what we observed to take place with a time constant of $\tau_1 = 6.5 \text{ ns}$, a transition that is followed by the Fe-His bond cleavage. As shown in Figs. 3 and 4, the subsequent conversion 6c-NO \rightarrow distal 5c-NO does not depend upon NO concentration ($\tau_2 = 0.6 \mu\text{s}$ at both $20 \mu\text{M}$ and $200 \mu\text{M}$ NO), in accord with the fact that another NO molecule cannot diffuse from solution in this short time range, so that the 5c-NO species formed with τ_2 must remain distal. Should a conversion to a proximal 5c-NO species occur after τ_2 with binding of NO from solution, it would take place on a longer time range and in a diffusion-controlled manner.

The induced absorption at 100 ps corresponds to the static 5c-His spectrum above $\sim 430 \text{ nm}$ (Fig. 2D). However, this fact does not mean that the photolyzed sGC has already relaxed to the allosteric resting state, because the Soret absorption evolution probes, *stricto sensu*, the coordination changes of the heme iron (or changes of the heme planarity). We emphasize with this experiment that the recovery of the 5c-His sGC state is not equivalent to the recovery of the allosteric resting state, in which the cGMP synthesis is inhibited.

The 4c heme is a highly reactive species, as evidenced by the rates of NO and His¹⁰⁵ recombination ($1.3 \times 10^{11} \text{ s}^{-1}$ and $1.4 \times 10^{10} \text{ s}^{-1}$, respectively). Because it has been shown that the position of the heme Fe atom does not have an impact on the rate of NO geminate rebinding, either to the 4c heme (28) or to the 5c-His heme (31), we attribute this high reactivity to its electronic configuration. Indeed, our transient Raman spectroscopy studies have suggested that the 4c transient heme is a high-spin species with single-electron occupancy of both $d(z^2)$ and $d(x^2 - y^2)$ orbitals (28). Whereas NO geminate rebinding experiences no energy barrier, the very small energy barrier for His¹⁰⁵ rebinding is most probably due to the rotation of the side chain, which accounts for the 10-fold larger time constant $\tau_{\text{His}} = 70 \text{ ps}$. The fact that the ratio of NO and His rebinding is not determined by their respective kinetic constants indicates that they do not,

Table 1. Time constants and rates of the transitions measured in Figs. 2–4

Transitions	Lifetimes	Rates
Bimolecular NO binding to 5c-His		
[NO] = 20 μM	$\tau_3 = 250 \mu\text{s}$	$k_{6c} = 2 \times 10^8 \text{ M}^{-1} \cdot \text{s}^{-1}$
[NO] = 200 μM	$\tau_3 = 50 \mu\text{s}$	$k_{6c} = 1 \times 10^8 \text{ M}^{-1} \cdot \text{s}^{-1}$
Conversion 6c-NO \rightarrow 5c-NO		
[NO] = 20 μM	$\tau_4 = 43 \text{ ms}$	$k_{5c} = 1.15 \times 10^6 \text{ M}^{-1} \cdot \text{s}^{-1}$
[NO] = 200 μM	$\tau_4 = 10 \text{ ms}$	$k_{5c} = 0.5 \times 10^6 \text{ M}^{-1} \cdot \text{s}^{-1}$
Geminate NO rebinding to 5c-His	$\tau_1 = 6.5 \text{ ns}$	$k'_G = 0.15 \times 10^9 \text{ s}^{-1}$
Conversion 6c*-NO \rightarrow 5c*-NO	$\tau_2 = 0.66 \mu\text{s}$	$k'_{5c} = 1.5 \times 10^6 \text{ s}^{-1}$
His rebinding to 4c heme	$\tau_{\text{His}} = 70 \text{ ps}$	$k_{\text{His}} = 1.4 \times 10^{10} \text{ s}^{-1}$
Geminate NO rebinding to 4c heme	$\tau_{\text{gem}} = 7.5 \text{ ps}$	$k_{\text{gem}} = 0.13 \times 10^{12} \text{ s}^{-1}$
Structural transition sGC* \rightarrow sGC	$1 \mu\text{s} < \tau_R < 50 \mu\text{s}$	$2 \times 10^4 \text{ s}^{-1} < k_R < 10^6 \text{ s}^{-1}$

All values are measured at 20 °C.

*Activated form of sGC. The indices of time constants refer to the measured values, and the indices of rates refer to the processes detailed in Fig. 5.

strictly speaking, compete for binding to the heme. This observation is in accord (albeit not a proof) with NO binding to the proximal heme side (33, 34, 37), implying that NO must leave the heme pocket to release steric hindrance preventing His rebinding, which is controlled by a rotational energy barrier.

After the 5c-His heme is reformed, the subsequent NO rebinding occurs two orders of magnitude more slowly ($\tau_1 = 6.5$ ns) without any component in the 100- to 200-ps time range, as found for the globin family (31), or in the 200- to 400-ps time range for endothelial NO-synthase (38). However, nanosecond NO rebinding components were already observed in the case of NO-synthase (38) and have been assigned to NO already present within the protein access pathway from solvent. In line with this previous result, we assign the 6.5-ns component reported here to NO that has moved out of the sGC heme pocket but has remained within the access pathway between heme and solvent. All observed coordination transitions are summarized in a model of heme dynamics in Fig. 5.

We captured here the primary formation of 6c-NO from the resting state 5c-His sGC in 50–250 μ s, which has escaped detection so far. We must emphasize that in such measurements performed over nine orders of time magnitude, the geminate and bimolecular processes do not probe the same population of molecules, so that the resting state 5c-His does not appear for the geminate population.

Detection of NO Binding to the Proximal Heme Side. After binding of NO from solution to form the 6c-NO species (Fig. 5B), the cleavage of the Fe-His bond is concentration-dependent (16, 39) (Figs. 3 and 4). This fact led to the proposal that a second NO molecule may interact with the formed 5c-NO heme. Indeed, since the discovery by X-ray crystallography that NO binds to the

proximal heme side in AXCP (*Alcaligenes xylosoxidans* cytochrome *c'*) (37), numerous models of guanylate cyclase activation have been proposed, which include the binding of NO to the proximal heme side (16–21, 36) despite the fact that it has escaped direct observation so far in sGC. Recently, the structure of a bacterial domain H-NOX in a nitrosylated state has been resolved with NO bound to the proximal side (40), which reinforces the hypothesis of proximal binding in sGC. Contrastingly, only one experiment to date, based on EPR and isotopic NO detection (34), has provided an indication that this proximal location for NO may indeed occur in sGC, even though, after the fast geminate rebinding in the picosecond range, we did not assign any of the four subsequent transitions to proximal binding because of their spectral characteristics. However, we must discuss this possibility and assess how it may be integrated into our present picture.

One nanosecond after NO dissociation, only two species remain: the reformed 5c-NO (Fig. 5C) due to picosecond NO geminate recombination and 5c-His due to His rebinding (Fig. 5E), with both being formed with the 4c heme as an intermediate. Due to the high reactivity of the 4c heme, NO geminate rebinding is ultrafast (7.5 ps) and necessarily occurs to the same heme side from which NO was photodissociated (it is not known whether it is distal or proximal). As for the 5c-His heme, it leads to the 6c-NO species (Fig. 5E and F) either by geminate rebinding (6.5 ns) or by bimolecular rebinding (50–250 μ s; Fig. 5A and B), followed by Fe-His¹⁰⁵ bond breaking by *trans*-effect (0.66 μ s and 10–43 ms, respectively). Due to its NO concentration dependency, the proximal NO binding to the distal 5c-NO species (hypothetically replacing His¹⁰⁵) is limited by diffusion and would occur in the time range of 0.1 μ s to 0.1 ms (i.e., the window between the geminate and bimolecular

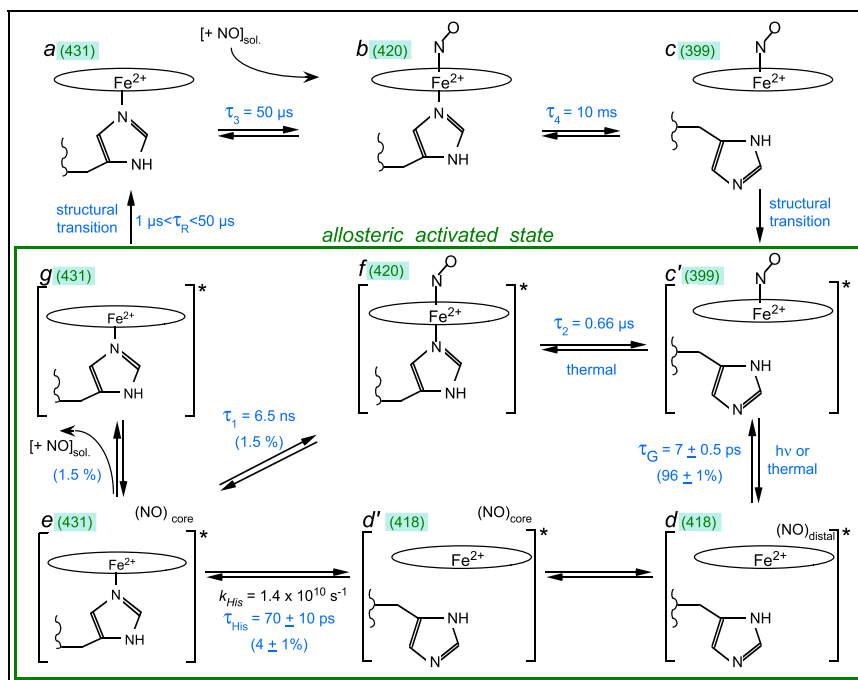


Fig. 5. Model describing the species involved in these experiments. The species involved are 5c-His sGC in the resting state (A); 6c-NO sGC in the resting state (B); 5c-NO sGC (C); 5c-NO sGC in the activated state (C'); 4c sGC after NO dissociation (D); 5c-His sGC in the activated state, immediately after His¹⁰⁵ rebinding (E); 6c sGC in the activated state, immediately after NO geminate rebinding (F); and 5c-His sGC in the activated state, with NO having left the protein core (G). The value highlighted in green adjacent to the letter label is the Soret maximum wavelength of the species, and the asterisk at the right bracket denotes the activated state of sGC (in the green box). The starting species of the kinetic measurements is shown in C. The time constants indicated are those time constraints measured in the present experiments. The corresponding rates are indicated in Table 1. In D, NO is located within the heme pocket, whereas in D' and E, NO is located in another docking site in the protein. The proximal NO binding is not included here but could easily be added to this model. The time constants τ_3 and τ_4 depend upon NO concentration and are indicated for [NO] = 200 μ M.

rebindings, during which no supplementary phase was detected) (Fig. 3 C and D).

In AXCP, the proximal 5c-NO complex forms via a dissociative mechanism with a dinitrosyl intermediate species formed after the dissociation of proximal His (39). Both distal and proximal NO-heme should have the same absorption spectrum and cannot be distinguished, so that the process could be detected by electronic absorption only by probing the transient dinitrosyl heme [heme]-(NO)₂. The equilibrium [heme]-NO + NO \leftrightarrow [heme]-(NO)₂ has a dissociation constant of ~ 2 M at 298 K (39, 41), so that the dinitrosyl species have a very short lifetime at low [NO], certainly smaller than 0.1 ms, which remains to be measured independently. This short dinitrosyl lifetime would preclude distinguishing it from the formation of the distal 5c-NO (10 ms) associated with the slow Fe-His bond breaking. It would thus escape detection, and so would the proximal 5c-NO formation after bimolecular rebinding.

On the other hand, 6c-NO is formed in 6.5 ns by geminate rebinding. Can we detect dinitrosyl heme from this process? Because this process would involve a second NO molecule from the solution, it is unlikely to occur with such a fast rate. The Soret absorption spectra of dinitrosyl porphyrins were observed only in organic solvents (41, 42) with a maximum at 416–418 nm ($\epsilon = 140 \times 10^3 \text{ M}^{-1}\text{cm}^{-1}$), clearly separated from other species (42, 43). Albeit the maximum can be shifted in organic solvents with respect to water buffer, additional kinetic components would be expected if a dinitrosyl heme intermediate were involved. However, the kinetics reported here disclose only two phases, whose amplitudes have a wavelength dependency inconsistent with the dinitrosyl formation or decay. No components can be directly attributed to transient dinitrosyl, leading to the conclusion that proximal NO binding to sGC, replacing His¹⁰⁵, is not detected in these kinetics. In brief, the decay of dinitrosyl, if it exists, is probably much faster than its formation, making it impossible to detect directly after NO diffusion from solvent. Our data can be entirely accounted for by a one-site model of heme dynamics (Fig. 5), and there is no need to include the hypothetical NO proximal binding.

In any case, should NO proximal binding occur at a larger NO concentration, it would imply that the rebinding of His¹⁰⁵ creates a kinetic gate, as demonstrated in the case of bacterial cytochrome *c'* (30). In that case, NO could not rebind geminately to the heme once it has moved out of the heme proximal pocket, contrary to distal binding. A very strong implication of the proximal binding is that the deactivation process is mechanistically different at low and high NO concentrations.

Structural Allosteric Transition. An important observation reported here is that the same coordination transition, the cleavage of the Fe-His bond, takes place with two very different time constants (Fig. 5 B and C vs. F and C). Either NO geminate rebinding from within the heme pocket to the 5c heme ($\tau_{G2} = 6.5$ ns) forming a 6c-NO intermediate with subsequent cleavage of the Fe-His bond ($\tau_{5C1} = 0.66$ μ s) or NO binding after diffusion from the solution ($\tau_{5C2} = 10$ ms with 200 μ M) leads eventually to the formation of 5c-NO heme. The mere fact that the conversion 6c-NO \rightarrow 5c-NO can take place with very different time constants (0.66 μ s and 10 ms) implies that the conformation of the protein is different in both cases. In other terms, the species 6c-NO can adopt two states that differ in their energy and structural constraints, showing that a structural relaxation occurred between both, which corresponds to the allosteric transition between the resting state and the activated state, leading to cGMP synthesis. This transition of sGC occurs in the time range of $1 \mu\text{s} < \tau_R < 50 \mu\text{s}$ (considering the lower limit reached when [NO] = 200 μ M) between geminate and bimolecular rebinding of NO, and similarly with CO, whose dynamics are influenced by the allosteric state of sGC (44).

After NO release from the heme, even if the Fe-His bond has been reformed, sGC remains in the activated state for a few microseconds and its conformation is such that the strains exerted on His¹⁰⁵ considerably facilitate the Fe-His bond cleavage if NO rebinds in the distal position, rendering the NO *trans*-effect more efficient. The structure of the activated state favors the release of proximal His with respect to the resting state. Conversely, the larger time constant for Fe-His bond cleavage indicates a less efficient *trans*-effect due to lower structural strains on His¹⁰⁵ in the resting state. The activation and deactivation of sGC do not follow the same time constants as His¹⁰⁵ rebinding, and heme coordination changes due to energy barriers for tertiary and quaternary changes. This conformational transition involves parts of all domains within both subunits of sGC, as demonstrated by hydrogen-deuterium exchange analysis (15).

By analogy with hemoglobin (45, 46), the allosteric states of sGC can be named as “relaxed” (R) and “tensed” (T), respectively. In the T state of hemoglobin, the constraints within the protein structure were also demonstrated via the Fe-His bond, in conditions where it could be broken upon diatomic binding (47). Remarkably, the time range that we have inferred for the allosteric transition in sGC (1–50 μ s) corresponds to the time constant of the R \leftrightarrow T allosteric transition in tetrameric hemoglobin measured by electronic transient absorption (10–20 μ s) probing the heme level (48, 49), by time-resolved Raman spectroscopy (17 μ s) probing aromatic side chains (50), or by transient X-ray scattering (2 μ s) probing the quaternary and tertiary overall structure (51). The allosteric transition was also demonstrated for a dimeric hemoglobin in the time range of 1–80 μ s by transient X-ray crystallography (52), whereas a 20- μ s relaxation of the polypeptide chain was also probed by IR absorption in nonheme protein (53). Thus, the allosteric transitions appear generally to reside in this early microsecond time range.

In summary, the measurement of heme coordination changes over 11 temporal decades allowed us to identify the time range of allosteric transition in sGC and to demonstrate that NO cannot bind from solution to the 4c heme because of the His¹⁰⁵ rebinding in 70 ps, which is almost energy-barrierless. This proximal histidine binding provokes a kinetic gate four orders of temporal magnitude faster than the cleavage of the Fe-His bond by NO *trans*-effect in the activated state of sGC.

Materials and Methods

Purification of sGC and Sample Preparation. sGC was purified from beef lung, and its activity was assayed as previously described (25). sGC was obtained directly in the ferrous state after the last column ($\lambda_{\text{max}} = 432$ nm; Fig. 2A). The final buffer was 25 mM TEA (triethanolamine), 50 mM NaCl, 1 mM DTT (dithiothreitol), and 1 mM MgCl₂ at pH 7.4. An aliquot of sGC in buffer (70 μ L at ~ 20 μ M) was put in a 1-mm optical pathlength quartz cell (110-QX; Hellma) sealed with a rubber stopper, and degassed with four cycles of vacuuming and purging with argon (99.999%; Air Liquide). For preparing NO-liganded sGC, 1% NO or 10% (vol/vol) diluted in N₂ (Air Liquide) was directly introduced in the vacuumed spectroscopic cell through the gas train, yielding 20 μ M NO in the aqueous phase. A second stopper in silicone, with vacuum grease, was stacked on the cell. Steady-state absorption spectra (UV-1700 spectrophotometer; Shimadzu) were recorded for monitoring the evolution of NO binding and after the laser measurements to verify the state of the sample. The absorbance of the nitrosylated sGC samples was in the range of 0.2–0.3 at the maximum of the Soret band.

Picosecond Time-Resolved Absorption (1 ps to 5 ns). Time-resolved picosecond absorption was performed using the pump-probe laser system previously described (54). The photodissociation of NO was achieved with an excitation pulse at 564 nm whose duration was ~ 40 fs with a repetition rate of 30 Hz. The broad-spectrum probe pulse was generated by means of a continuum. The transient absorption spectrum after a variable delay between pump and probe pulses was recorded with a CCD detector coupled to a spectrometer. The same sample quartz cell (1-mm optical pathlength) was used for recording the equilibrium spectra and the transient absorption. The temperature was 18 $^{\circ}$ C during all measurements. Up to 50 scans were averaged.

Transient spectra were recorded simultaneously with kinetics as a time-wavelength matrix, and the decay of heme electronic excited states was taken into account (54). Kinetics at individual wavelengths were fitted to the sum of a minimum number of exponential components.

Nanosecond to Millisecond Time-Resolved Absorption (5 ns to 0.3 s). For this extended time range, we have used a home-built spectrophotometer comprising two lasers, which are electronically delayed (32). The dissociating pulse is provided by the second harmonic (532 nm) of a neodymium-doped yttrium aluminium garnet (Nd:YAG) laser and has a duration of 6 ns. The probing pulses (6 ns at FWHM) were provided by a tunable optical parametric oscillator pumped by the third harmonic of an Nd:YAG laser (Continuum). The sample cell compartment and light collection design allowed us

to record signal variations of $\Delta\text{OD}/\text{OD} < 10^{-5}$. The kinetics of differential absorption changes were probed at particular wavelengths by tuning the OPO (optical parametric oscillator). Four scans were averaged for each kinetic value. Time delays after the dissociating pulse were changed linearly from 1 to 30 ns and were then changed with a logarithmic progression from 30 ns to 0.2 s. The kinetics at different wavelengths were globally fitted by using the same time constants.

ACKNOWLEDGMENTS. We thank Prof. Ah-Lim Tsai and Prof. Colin Andrew for stimulating discussions. B.-K.Y. was supported by the Fondation pour la Recherche Médicale. M.N. received financial support from INSERM. F.R. acknowledges financial support from the CNRS and the "Initiative d'Excellence" program from the French state (Grant "DYNAMO," ANR-11-LABX-0011-01).

- Ignarro LJ, Buga GM, Wood KS, Byrns RE, Chaudhuri G (1987) Endothelium-derived relaxing factor produced and released from artery and vein is nitric oxide. *Proc Natl Acad Sci USA* 84(24):9265–9269.
- Palmer RMJ, Ferrige AG, Moncada S (1987) Nitric oxide release accounts for the biological activity of endothelium-derived relaxing factor. *Nature* 327(6122):524–526.
- Bian K, Doursout MF, Murad F (2008) Vascular system: Role of nitric oxide in cardiovascular diseases. *J Clin Hypertens (Greenwich)* 10(4):304–310.
- Coggins MP, Bloch KD (2007) Nitric oxide in the pulmonary vasculature. *Arterioscler Thromb Vasc Biol* 27(9):1877–1885.
- Nagy G, Clark JM, Buzás EI, Gorman CL, Cope AP (2007) Nitric oxide, chronic inflammation and autoimmunity. *Immunol Lett* 111(1):1–5.
- Blaise GA, Gauvin D, Gangai M, Authier S (2005) Nitric oxide, cell signaling and cell death. *Toxicology* 208(2):177–192.
- Evgenov OV, et al. (2006) NO-independent stimulators and activators of soluble guanylate cyclase: Discovery and therapeutic potential. *Nat Rev Drug Discov* 5(9):755–768.
- Stasch JP, Pacher P, Evgenov OV (2011) Soluble guanylate cyclase as an emerging therapeutic target in cardiopulmonary disease. *Circulation* 123(20):2263–2273.
- Mittendorf J, et al. (2009) Discovery of riociguat (BAY 63-2521): A potent, oral stimulator of soluble guanylate cyclase for the treatment of pulmonary hypertension. *ChemMedChem* 4(5):853–865.
- Follmann M, et al. (2013) The chemistry and biology of soluble guanylate cyclase stimulators and activators. *Angew Chem Int Ed Engl* 52(36):9442–9462.
- Nioche P, et al. (2004) Femtomolar sensitivity of a NO sensor from *Clostridium botulinum*. *Science* 306(5701):1550–1553.
- Pellicena P, Karow DS, Boon EM, Marletta MA, Kuriyan J (2004) Crystal structure of an oxygen-binding heme domain related to soluble guanylate cyclases. *Proc Natl Acad Sci USA* 101(35):12854–12859.
- Liu Y, Ruoho AE, Rao VD, Hurler JH (1997) Catalytic mechanism of the adenyllyl and guanylyl cyclases: Modeling and mutational analysis. *Proc Natl Acad Sci USA* 94(25):13414–13419.
- Campbell MG, Underbakke ES, Potter CS, Carragher B, Marletta MA (2014) Single-particle EM reveals the higher-order domain architecture of soluble guanylate cyclase. *Proc Natl Acad Sci USA* 111(8):2960–2965.
- Underbakke ES, et al. (2014) Nitric oxide-induced conformational changes in soluble guanylate cyclase. *Structure* 22(4):602–611.
- Zhao Y, Brandish PE, Ballou DP, Marletta MA (1999) A molecular basis for nitric oxide sensing by soluble guanylate cyclase. *Proc Natl Acad Sci USA* 96(26):14753–14758.
- Russwurm M, Koesling D (2004) NO activation of guanylyl cyclase. *EMBO J* 23(22):4443–4450.
- Pal B, Kitagawa T (2005) Interactions of soluble guanylate cyclase with diatomics as probed by resonance Raman spectroscopy. *J Inorg Biochem* 99(1):267–279.
- Poulos TL (2006) Soluble guanylate cyclase. *Curr Opin Struct Biol* 16(6):736–743.
- Ma X, Sayed N, Beuve A, van den Akker F (2007) NO and CO differentially activate soluble guanylyl cyclase via a heme pivot-bend mechanism. *EMBO J* 26(2):578–588.
- Cary SPL, Winger JA, Derbyshire ER, Marletta MA (2006) Nitric oxide signaling: No longer simply on or off. *Trends Biochem Sci* 31(4):231–239.
- Garthwaite J (2010) New insight into the functioning of nitric oxide-receptive guanylyl cyclase: Physiological and pharmacological implications. *Mol Cell Biochem* 334(1-2):221–232.
- Tsai AL, Berka V, Sharina I, Martin E (2011) Dynamic ligand exchange in soluble guanylyl cyclase (sGC): Implications for sGC regulation and desensitization. *J Biol Chem* 286(50):43182–43192.
- Stone JR, Marletta MA (1994) Soluble guanylate cyclase from bovine lung: Activation with nitric oxide and carbon monoxide and spectral characterization of the ferrous and ferric states. *Biochemistry* 33(18):5636–5640.
- Négrerie M, Bouzahir L, Martin JL, Liebl U (2001) Control of nitric oxide dynamics by guanylate cyclase in its activated state. *J Biol Chem* 276(50):46815–46821.
- Yoo BK, Lamarre I, Martin JL, Négrerie M (2012) Quaternary structure controls ligand dynamics in soluble guanylate cyclase. *J Biol Chem* 287(9):6851–6859.
- Martin E, Berka V, Tsai AL, Murad F (2005) Soluble guanylyl cyclase: The nitric oxide receptor. *Methods Enzymol* 396:478–492.
- Kruglik SG, et al. (2007) Molecular basis for nitric oxide dynamics and affinity with *Alcaligenes xylosoxidans* cytochrome c. *J Biol Chem* 282(7):5053–5062.
- Benabbas A, et al. (2010) Ultrafast dynamics of diatomic ligand binding to nitrophorin 4. *J Am Chem Soc* 132(8):2811–2820.
- Yoo BK, Lamarre I, Martin JL, Andrew CR, Négrerie M (2013) Picosecond binding of the His ligand to four-coordinate heme in cytochrome c: A one-way gate for releasing proximal NO. *J Am Chem Soc* 135(8):3248–3254.
- Kruglik SG, et al. (2010) Picosecond primary structural transition of the heme is retarded after nitric oxide binding to heme proteins. *Proc Natl Acad Sci USA* 107(31):13678–13683.
- Beal D, Rappaport F, Joliet P (1999) A new high-sensitivity 10-ns time-resolution spectrophotometric technique adapted to in vivo analysis of the photosynthetic apparatus. *Rev Sci Instrum* 70(1):202–207.
- Andrew CR, Rodgers KR, Eady RR (2003) A novel kinetic trap for NO release from cytochrome c: A possible mechanism for NO release from activated soluble guanylate cyclase. *J Am Chem Soc* 125(32):9548–9549.
- Martin E, Berka V, Sharina I, Tsai AL (2012) Mechanism of binding of NO to soluble guanylyl cyclase: Implication for the second NO binding to the heme proximal site. *Biochemistry* 51(13):2737–2746.
- Roy B, Garthwaite J (2006) Nitric oxide activation of guanylyl cyclase in cells revisited. *Proc Natl Acad Sci USA* 103(32):12185–12190.
- Halvey EJ, Vernon J, Roy B, Garthwaite J (2009) Mechanisms of activity-dependent plasticity in cellular nitric oxide-cGMP signaling. *J Biol Chem* 284(38):25630–25641.
- Lawson DM, Stevenson CEM, Andrew CR, Eady RR (2000) Unprecedented proximal binding of nitric oxide to heme: Implications for guanylate cyclase. *EMBO J* 19(21):5661–5671.
- Négrerie M, et al. (1999) Geminate recombination of nitric oxide to endothelial nitric oxide synthase and mechanistic implications. *J Biol Chem* 274(35):24694–24702.
- Pixton DA, et al. (2009) Activation parameters for heme-NO binding in alcaligenes xylosoxidans cytochrome c: The putative dinitrosyl intermediate forms via a dissociative mechanism. *J Am Chem Soc* 131(13):4846–4853.
- Herzik MA, Jr, Jonnalagadda R, Kuriyan J, Marletta MA (2014) Structural insights into the role of iron-histidine bond cleavage in nitric oxide-induced activation of H-NOX gas sensor proteins. *Proc Natl Acad Sci USA* 111(40):E4156–E4164.
- Lorkovic IM, Ford PC (2000) Nitric oxide addition to the ferrous nitrosyl porphyrins Fe(P)(NO) gives trans-Fe(P)(NO)₂ in low-temperature solutions. *J Am Chem Soc* 122(27):6516–6517.
- Wayland BB, Olson LW (1974) Spectroscopic studies and bonding model for nitric oxide complexes of iron porphyrins. *J Am Chem Soc* 96(19):6037–6041.
- Lim MD, Lorkovic IM, Ford PC (2005) NO and NO_x interactions with group 8 metal-porphyrins. *J Inorg Biochem* 99(1):151–165.
- Yoo BK, et al. (2012) Picosecond to second dynamics reveals a structural transition in *Clostridium botulinum* NO-sensor triggered by the activator BAY-41-2272. *ACS Chem Biol* 7(12):2046–2054.
- Perutz MF (1970) Stereochemistry of cooperative effects in haemoglobin. *Nature* 228(5273):726–739.
- Perutz MF, Wilkinson AJ, Paoli M, Dodson GG (1998) The stereochemical mechanism of the cooperative effects in hemoglobin revisited. *Annu Rev Biophys Biomol Struct* 27:1–34.
- Paoli M, Dodson G, Liddington RC, Wilkinson AJ (1997) Tension in haemoglobin revealed by Fe-His(F8) bond rupture in the fully liganded T-state. *J Mol Biol* 271(2):161–167.
- Hofrichter J, Sommer JH, Henry ER, Eaton WA (1983) Nanosecond absorption spectroscopy of hemoglobin: Elementary processes in kinetic cooperativity. *Proc Natl Acad Sci USA* 80(8):2235–2239.
- Jones CM, et al. (1992) Speed of intersubunit communication in proteins. *Biochemistry* 31(29):6692–6702.
- Jayaraman V, Rodgers KR, Mukerji I, Spiro TG (1995) Hemoglobin allostery: Resonance Raman spectroscopy of kinetic intermediates. *Science* 269(5232):1843–1848.
- Cammarata M, Levantino M, Wulff M, Cupane A (2010) Unveiling the timescale of the R-T transition in human hemoglobin. *J Mol Biol* 400(5):951–962.
- Knapp JE, Pahl R, Šrajer V, Royer WE, Jr (2006) Allosteric action in real time: Time-resolved crystallographic studies of a cooperative dimeric hemoglobin. *Proc Natl Acad Sci USA* 103(20):7649–7654.
- Buchli B, et al. (2013) Kinetic response of a photoperurbed allosteric protein. *Proc Natl Acad Sci USA* 110(29):11725–11730.
- Négrerie M, Cianetti S, Vos MH, Martin JL, Kruglik SG (2006) Ultrafast heme dynamics in ferrous versus ferric cytochrome c studied by time-resolved resonance Raman and transient absorption spectroscopy. *J Phys Chem B* 110(25):12766–12781.